

On Inverse Form Finding for Anisotropic Hyperelasticity in Logarithmic Strain Space

Sandrine Germain, Michael Scherer, and, Paul Steinmann¹

Chair of Applied Mechanics, University of Erlangen/Nuremberg, Germany

Abstract

The goal of this contribution is to extend the work of Govindjee and Mihalic (1996) on inverse form finding for isotropic hyperelastic materials to the case of anisotropic hyperelastic materials formulated in the logarithmic strain space. A review of the pertinent theoretical aspects is presented. This is followed by several detailed numerical examples which highlight key features of the algorithm.

Key words: Anisotropy; Logarithmic Strain; Inverse Form Finding; Large Strain

1. Introduction

A challenge in the design of functional parts is the determination of the initial, undeformed shape such that under a given load a part will obtain the desired deformed shape. This is an inverse form finding problem and is posed as follows: given the spatial configuration, i.e. the deformed shape and the mechanical loading, find the inverse deformation map that determines the material configuration, i.e. the undeformed shape. This problem is inverse to the standard (direct) elastostatic analysis in which the undeformed shape is known and the deformed unknown. A numerical procedure for the determination of the undeformed shape of a continuous body has been proposed in Govindjee and Mihalic (1996) and Govindjee and Mihalic (1998). Their work is restricted to isotropic compressible neo-Hookean and incompressible materials, respectively. One result of their work is that the weak form of the inverse motion problem based on the Cauchy stress is more efficient and straightforward as compared to the weak form based on the Eshelby stress (energy momentum tensor). The governing equation underlying the numerical analysis of the inverse form finding problem is therefore, surprisingly, the common weak form of the balance of momentum formulated in terms of the Cauchy stress tensor. However, the unconventional issue is that all quantities are parameterized in the spatial coordinates. Later, Fachinotti et al. (2008) extended this method to the case of anisotropic hyperelasticity for a St.Venant type material, i.e. a material characterized by a quadratic free energy density in terms of the Green-Lagrange strain. The consideration of temperature changes in the undeformed and deformed configuration has been included in Govindjee (1999) for orthotropic nonlinear elasticity and axisymmetry using a St.Venant type material. An application has been developed in Koishi and Govindjee (2001) for the purpose of tire design. In this contribution, we further extend the method originally proposed in Govindjee and Mihalic (1996) to anisotropic hyperelasticity that is based on logarithmic (Hencky) strains. The governing equation for the resulting finite element analysis is the weak form of the balance of momentum formulated in terms of the deformed configuration using the Cauchy stress tensor. The anisotropic free energy density is expressed as a quadratic function of the logarithmic strain and a constant anisotropic stiffness tensor. The motivation for the use of the logarithmic strain space formulation is that it mimics the small strain format and the corresponding fourth-order stiffness tensor is known for many symmetry classes of anisotropic materials.

Email address: paul.steinmann@ltm.uni-erlangen.de (Paul Steinmann)

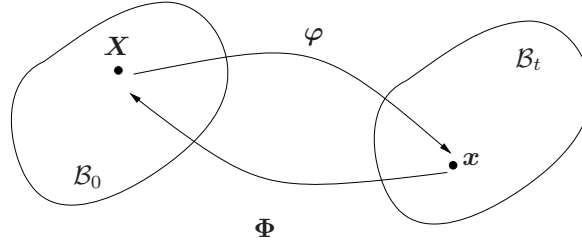


Figure 1: Spatial motion.

The paper is organised as follows: in section 2, we briefly present the kinematics of the direct and the inverse problems. Section 3 summarizes anisotropic elasticity in the logarithmic strain space. In section 4, we review the ordinary direct problem to determine the deformed shape based on the knowledge of the undeformed shape. Section 5 presents the corresponding inverse problem that determines the undeformed shape based on knowledge of the deformed shape. The finite element discretization of the direct and the inverse problem is described in section 6. In section 7, we present various representative numerical examples for the inverse form finding in anisotropic hyperelasticity.

2. Kinematics of Geometrically Nonlinear Continuum Mechanics

To set the stage, we briefly recall the basic kinematic quantities of geometrically nonlinear continuum mechanics. Let \mathcal{B}_0 denote the material configuration (the undeformed shape) of a continuum body parameterized by material coordinates \mathbf{X} and \mathcal{B}_t the corresponding spatial configuration (the deformed shape) parameterized by spatial coordinates \mathbf{x} , as depicted in Figure 1. In the direct problem, the material configuration is given and we seek to determine the (direct) deformation map φ as

$$\mathbf{x} = \varphi(\mathbf{X}) : \mathcal{B}_0 \longrightarrow \mathcal{B}_t. \quad (1)$$

The corresponding linear tangent map or rather the (direct) deformation gradient together with its Jacobian determinant are defined as

$$\mathbf{F} = \nabla_{\mathbf{X}} \varphi, \quad J = \det \mathbf{F}. \quad (2)$$

Here $\nabla_{\mathbf{X}}$ denotes the gradient operator with respect to the material coordinates \mathbf{X} . On the contrary, in the inverse problem, the spatial configuration is given and we seek to determine the inverse deformation map Φ as

$$\mathbf{X} = \Phi(\mathbf{x}) : \mathcal{B}_t \longrightarrow \mathcal{B}_0. \quad (3)$$

The corresponding linear tangent map or rather the inverse deformation gradient together with its Jacobian determinant are given by

$$\mathbf{f} = \nabla_{\mathbf{x}} \Phi, \quad j = \det \mathbf{f}. \quad (4)$$

Here $\nabla_{\mathbf{x}}$ denotes the gradient operator with respect to the spatial coordinates \mathbf{x} . It follows immediately from the above definitions that the inverse deformation map denotes a (nonlinear) map inverse to the deformation map of the direct problem

$$\Phi = \varphi^{-1}. \quad (5)$$

Thus the inverse and (direct) deformation gradients together with their Jacobian determinants are simply related through an algebraic inversion

$$\mathbf{f} = \mathbf{F}^{-1}, \quad j = J^{-1}. \quad (6)$$

3. Anisotropic Elasticity in Logarithmic Strain Space

In this section we mainly summarize the exposition in Miehe and Lambrecht (2001) to facilitate the subsequent presentation. A valid model option for anisotropic finite strain hyperelasticity is a quadratic free energy density per unit volume in \mathcal{B}_0

$$\psi_0 = \psi_0(\mathbf{E}) = \frac{1}{2} \mathbf{E} : \mathbb{E} : \mathbf{E} \quad (7)$$

in terms of the second-order logarithmic strain tensor

$$\mathbf{E} = \frac{1}{2} \ln \mathbf{C} \quad (8)$$

and a constant anisotropic fourth-order stiffness tensor

$$\mathbb{E} = E_{IJKL} \mathbf{E}_I \otimes \mathbf{E}_J \otimes \mathbf{E}_K \otimes \mathbf{E}_L = E_{MNOP}^0 \mathbf{E}_M^0 \otimes \mathbf{E}_N^0 \otimes \mathbf{E}_O^0 \otimes \mathbf{E}_P^0. \quad (9)$$

Here E_{MNOP}^0 denote the (known) coefficients of the anisotropic stiffness tensor in a coordinate system intrinsic to the material with orthonormal base vectors \mathbf{E}_M^0 . These in turn are given by a forward rotation from the base vectors \mathbf{E}_M of the laboratory coordinate system

$$\mathbf{E}_M^0 = \mathbf{Q} \cdot \mathbf{E}_M = Q_{IM} \mathbf{E}_I, \quad \text{with} \quad \mathbf{Q} = Q_{IJ} \mathbf{E}_I \otimes \mathbf{E}_J \in \text{SO}(3). \quad (10)$$

As a consequence the coefficients of the anisotropic stiffness tensor in the laboratory coordinate system follow as

$$E_{IJKL} = Q_{IM} Q_{JN} E_{MNOP}^0 Q_{KO} Q_{LP}. \quad (11)$$

As an example the orthotropy symmetry class is detailed in the appendix. The spectral decomposition of the right Cauchy–Green strain tensor \mathbf{C} reads

$$\mathbf{C} = \mathbf{F}^t \cdot \mathbf{F} = \sum_{i=1}^3 \lambda_i \mathbf{M}_i \quad (12)$$

with $\{\lambda_i\}_{i=1,2,3}$ the real eigenvalues of \mathbf{C} and $\{\mathbf{M}_i\}_{i=1,2,3}$ the associated eigenbases (Miehe (1993)). The spectral representation facilitates the computation of the logarithmic strain

$$\mathbf{E} = \frac{1}{2} \sum_{i=1}^3 \ln \lambda_i \mathbf{M}_i \quad (13)$$

and allows a closed form expression for the (first and second) derivatives of the logarithmic strain with respect to the right Cauchy–Green strain

$$\mathbb{P} = 2 \frac{\partial \mathbf{E}}{\partial \mathbf{C}} \quad \text{and} \quad \mathbb{L} = 2 \frac{\partial \mathbb{P}}{\partial \mathbf{C}} = 4 \frac{\partial^2 \mathbf{E}}{\partial \mathbf{C} \partial \mathbf{C}}. \quad (14)$$

For more details of how to compute these derivatives the interested reader is referred to Miehe and Lambrecht (2001).

Using (14), the Piola–Kirchhoff stress may be represented as

$$\mathbf{S} = 2 \frac{\partial \psi_0}{\partial \mathbf{C}} = \mathbf{T} : \mathbb{P} \quad \text{with} \quad \mathbf{T} = \frac{\partial \psi_0}{\partial \mathbf{E}} = \mathbb{E} : \mathbf{E}. \quad (15)$$

Considering this expression, the linearization of the Piola–Kirchhoff stress (tangent operator needed in a Newton type solution scheme) reads

$$\mathbb{C} = 4 \frac{\partial^2 \psi_0}{\partial \mathbf{C} \partial \mathbf{C}} = \mathbb{P}^T : \mathbb{E} : \mathbb{P} + \mathbf{T} : \mathbb{L} \quad \text{with} \quad \mathbb{E} = \frac{\partial^2 \psi_0}{\partial \mathbf{E} \partial \mathbf{E}}. \quad (16)$$

The transposition symbol $[\bullet]^T$ refers to an exchange of the first and last pairs of indices. Summarizing, the use of the logarithmic strain in an anisotropic model of finite strain hyperelasticity has several advantages:

- ψ_0 is a quadratic function in \mathbf{E} ,
- the anisotropic stiffness tensor \mathbb{E} is known for a wide range of symmetry classes; thus the formulation of anisotropic hyperelasticity is straightforward,
- in a nutshell it mimics the small strain format that is, however, modified by purely geometric, problem independent operators \mathbb{P} and \mathbb{L} .

4. Determining the Deformed Shape from Equilibrium

For the sake of presentation, we shall omit distributed body forces and inertia henceforth. The nonlinear deformation map $\varphi = \varphi(\mathbf{X})$ is determined for given \mathbf{X} by the requirement of equilibrium as embodied in the following boundary value problem

$$\begin{aligned} \text{Div}(\mathbf{F} \cdot \mathbf{S}) &= \mathbf{0} && \text{in } \mathcal{B}_0, \\ [\mathbf{F} \cdot \mathbf{S}] \cdot \mathbf{N} &= \bar{\mathbf{t}}_0 && \text{on } \partial\mathcal{B}_0^t, \\ \varphi &= \bar{\varphi} && \text{on } \partial\mathcal{B}_0^\varphi. \end{aligned} \quad (17)$$

Here $\bar{\mathbf{t}}_0$ is a prescribed (given) traction per unit area in the material configuration (Neumann data) and $\bar{\varphi}$ is a prescribed boundary deformation (Dirichlet data) and Div denotes the material divergence operator with respect to the material coordinates \mathbf{X} . Accordingly, the weak form of the given boundary value problem reads, with the test function $\boldsymbol{\eta} \in V_0 = \{\boldsymbol{\eta} \in H^1(\mathcal{B}_0) | \boldsymbol{\eta} = \mathbf{0} \text{ on } \partial\mathcal{B}_0^\varphi\}$, as

$$G(\varphi, \boldsymbol{\eta}; \mathbf{X}) = \int_{\mathcal{B}_0} [\mathbf{F}^t \cdot \nabla_{\mathbf{X}} \boldsymbol{\eta}] : \mathbf{S} \, dV - \int_{\partial\mathcal{B}_0^t} \boldsymbol{\eta} \cdot \bar{\mathbf{t}}_0 \, dA = 0 \quad \forall \boldsymbol{\eta} \in V_0. \quad (18)$$

Note that the above is the common virtual work statement with a parameterization of all quantities in the (given) material coordinates \mathbf{X} . For hyperelastostatics the (symmetric) Piola–Kirchhoff stress is expressed as a functional of $\varphi = \varphi(\mathbf{X})$ as

$$\mathbf{S} = \mathbf{S}(\nabla_{\mathbf{X}} \varphi(\mathbf{X})). \quad (19)$$

The corresponding linearization (directional derivative) of the weak form in the direction $\Delta\varphi$ at fixed material coordinates \mathbf{X} as needed in a Newton type solution scheme is finally expressed as

$$\frac{d}{d\epsilon} G(\varphi + \epsilon \Delta\varphi, \boldsymbol{\eta}; \mathbf{X})|_{\epsilon=0} = \int_{\mathcal{B}_0} \nabla_{\mathbf{X}} \boldsymbol{\eta} : \mathbb{A} : \Delta\mathbf{F} \, dV. \quad (20)$$

Here the fourth-order tangent operator \mathbb{A} decomposes into the material tangent operator \mathbb{C} (see (16)) and a geometrical contribution

$$\mathbb{A} := \frac{\partial[\mathbf{F} \cdot \mathbf{S}]}{\partial \mathbf{F}} = [\mathbf{F} \bar{\otimes} \mathbf{I}] : \mathbb{C} : [\mathbf{F}^t \bar{\otimes} \mathbf{I}] + \mathbf{i} \bar{\otimes} \mathbf{S}. \quad (21)$$

In the above expression \mathbf{I} and \mathbf{i} denote the material and spatial unit tensors with coefficients δ_{IJ} and δ_{ij} , respectively, $\bar{\otimes}$ denotes a non-standard dyadic product with $[\mathbf{A} \bar{\otimes} \mathbf{B}]_{IJKL} = A_{IK} B_{JL}$.

5. Determining the Undeformed Shape from Equilibrium

Alternatively, the equilibrium statement may be expressed by the following variant of the boundary value problem, here in terms of spatial description quantities

$$\begin{aligned} \text{div} \boldsymbol{\sigma} &= \mathbf{0} && \text{in } \mathcal{B}_t, \\ \boldsymbol{\sigma} \cdot \mathbf{n} &= \bar{\mathbf{t}}_t && \text{on } \partial\mathcal{B}_t^t, \\ \varphi &= \bar{\varphi} && \text{on } \partial\mathcal{B}_t^\varphi. \end{aligned} \quad (22)$$

Here $\bar{\mathbf{t}}_t$ is again the prescribed (given) traction, however now per unit area in the spatial configuration, and $\bar{\varphi}$ is the prescribed boundary deformation, div denotes the divergence operator with respect to the spatial coordinates \mathbf{x} . The (symmetric) Cauchy stress $\boldsymbol{\sigma}$ is obtained from the Piola–Kirchhoff stress by a push-forward according to

$$J\boldsymbol{\sigma} = \mathbf{F} \cdot \mathbf{S} \cdot \mathbf{F}^t. \quad (23)$$

The inverse form finding problem can be stated as follows: for a given spatial configuration, i.e. for a given deformed shape parameterized by the spatial coordinates \mathbf{x} , and associated boundary data, the material configuration, i.e. the undeformed shape with $\mathbf{X} = \Phi(\mathbf{x})$, satisfies the equilibrium requirement (22) for the spatial configuration.

Thus we now consider all quantities parameterized in the spatial coordinates \mathbf{x} . Accordingly, the weak form of the given boundary value problem, corresponding to the equilibrium requirement for the spatial configuration, reads

$$g(\Phi, \boldsymbol{\eta}; \mathbf{x}) = \int_{B_t} \nabla_{\mathbf{x}} \boldsymbol{\eta} : \boldsymbol{\sigma} \, dv - \int_{\partial B_t^i} \boldsymbol{\eta} \cdot \bar{\mathbf{t}}_t \, da = 0 \quad \forall \boldsymbol{\eta} \in V_0. \quad (24)$$

Clearly, equation (24) is the same virtual work statement as in (18), however all integrals extend now over the spatial configuration, that is here assumed given, and all quantities are parameterized in the given spatial coordinates \mathbf{x} . As an example the Piola–Kirchhoff stress \mathbf{S} is now expressed as a functional of the inverse deformation map $\mathbf{X} = \Phi(\mathbf{x})$

$$\mathbf{S} = \mathbf{S}([\nabla_{\mathbf{x}} \Phi(\mathbf{x})]^{-1}). \quad (25)$$

Since we now consider the spatial coordinates \mathbf{x} as fixed and since we want to determine the inverse deformation map $\mathbf{X} = \Phi(\mathbf{x})$ we need the linearization (directional derivative) of the weak form in the direction $\Delta \Phi$ at fixed spatial coordinates \mathbf{x}

$$\frac{d}{d\epsilon} g(\Phi + \epsilon \Delta \Phi, \boldsymbol{\eta}; \mathbf{x})|_{\epsilon=0} = \int_{B_t} \nabla_{\mathbf{x}} \boldsymbol{\eta} : \mathfrak{a} : \Delta \mathbf{f} \, dv. \quad (26)$$

The computation of the corresponding fourth-order tangent operator \mathfrak{a} simplifies considerably if we make the following assumptions:

1. the surface tractions per unit area in ∂B_t^i are given, i.e. they are independent of the inverse deformation map,
2. the material is homogeneous, i.e. $\boldsymbol{\sigma} = \boldsymbol{\sigma}(\mathbf{f}) \neq \boldsymbol{\sigma}(\mathbf{f}, \Phi)$.

With these assumptions \mathfrak{a} follows in a straightforward manner from the relation between the Cauchy and the Piola–Kirchhoff stresses and application of the chain and product rules of differentiation

$$\mathfrak{a} := \frac{\partial [j \mathbf{F} \cdot \mathbf{S} \cdot \mathbf{F}^t]}{\partial \mathbf{f}} = \boldsymbol{\sigma} \otimes \mathbf{F}^t - \mathbf{F} \bar{\otimes} \boldsymbol{\sigma} + j \mathbf{F} \cdot \left[\frac{1}{2} \mathbb{C} : \frac{\partial \mathbf{C}}{\partial \mathbf{f}} \right] \cdot \mathbf{F}^t - \boldsymbol{\sigma} \underline{\otimes} \mathbf{F}. \quad (27)$$

For the computation of the individual terms we make use of the following generic relations

$$\frac{\partial [\mathbf{A} \cdot \mathbf{B}]}{\partial \mathbf{A}} = \mathbf{I} \bar{\otimes} \mathbf{B}^t, \quad \frac{\partial [\mathbf{A} \cdot \mathbf{B}]}{\partial \mathbf{B}} = \mathbf{A} \bar{\otimes} \mathbf{I}, \quad (28)$$

together with the derivatives with respect to the inverse deformation gradient \mathbf{f}

$$\frac{\partial j}{\partial \mathbf{f}} = j \mathbf{F}^t, \quad \frac{\partial \mathbf{F}}{\partial \mathbf{f}} = -\mathbf{F} \bar{\otimes} \mathbf{F}^t, \quad \frac{\partial \mathbf{F}^t}{\partial \mathbf{f}} = -\mathbf{F}^t \underline{\otimes} \mathbf{F}. \quad (29)$$

With these preliminaries in hand the derivative of the right Cauchy–Green strain is expressed as

$$\frac{\partial \mathbf{C}}{\partial \mathbf{f}} = -\mathbf{F}^t \underline{\otimes} \mathbf{C} - \mathbf{C} \bar{\otimes} \mathbf{F}^t. \quad (30)$$

In the above, the non-standard dyadic product $\underline{\otimes}$ is defined by $[\mathbf{A} \underline{\otimes} \mathbf{B}]_{IJKL} = A_{IL} B_{JK}$, moreover the following useful relations holds

$$[\mathbf{A} \bar{\otimes} \mathbf{B}] : [\mathbf{C} \bar{\otimes} \mathbf{D}] = [\mathbf{A} \cdot \mathbf{C}] \bar{\otimes} [\mathbf{B} \cdot \mathbf{D}], \quad [\mathbf{A} \bar{\otimes} \mathbf{B}] : [\mathbf{C} \underline{\otimes} \mathbf{D}] = [\mathbf{A} \cdot \mathbf{C}] \underline{\otimes} [\mathbf{B} \cdot \mathbf{D}]. \quad (31)$$

6. Discretization and Solution Method

For the finite element solution of the two problems ((18) and (24)) the material and spatial solution domains \mathcal{B}_0 and \mathcal{B}_t are discretized into n_{el} elements

$$\mathcal{B}_0 \approx \mathcal{B}_0^h = \bigcup_{e=1}^{n_{el}} \mathcal{B}_0^e, \quad \mathcal{B}_t \approx \mathcal{B}_t^h = \bigcup_{e=1}^{n_{el}} \mathcal{B}_t^e. \quad (32)$$

Following the standard isoparametric approach, both, the geometry and the deformation maps are approximated on each element by the same shape functions

$$\begin{aligned} \mathbf{X}^e(\boldsymbol{\xi}) &= \sum_{i=1}^{n_{en}} \mathbf{X}^{(i)} N^{(i)}(\boldsymbol{\xi}), & \boldsymbol{\Phi}^e(\boldsymbol{\xi}) &= \sum_{i=1}^{n_{en}} \boldsymbol{\Phi}^{(i)} N^{(i)}(\boldsymbol{\xi}), \\ \mathbf{x}^e(\boldsymbol{\xi}) &= \sum_{i=1}^{n_{en}} \mathbf{x}^{(i)} N^{(i)}(\boldsymbol{\xi}), & \boldsymbol{\varphi}^e(\boldsymbol{\xi}) &= \sum_{i=1}^{n_{en}} \boldsymbol{\eta}^{(i)} N^{(i)}(\boldsymbol{\xi}). \end{aligned} \quad (33)$$

Thereby the shape functions $N^{(i)}$ are parameterized by isoparametric coordinates $\boldsymbol{\xi}$ defined on the isoparametric cube $\mathcal{B}^\xi = [-1, 1]^{n_{dim}}$, whereas n_{en} is the total number of nodes per element, and $\mathbf{X}^{(i)} = \boldsymbol{\Phi}^{(i)}$ and $\mathbf{x}^{(i)} = \boldsymbol{\varphi}^{(i)}$ denote nodal values. Finally, following the Bubnov–Galerkin method the test function is again approximated by the same shape functions $N^{(i)}$

$$\boldsymbol{\eta}^e(\boldsymbol{\xi}) = \sum_{i=1}^{n_{en}} \boldsymbol{\eta}^{(i)} N^{(i)}(\boldsymbol{\xi}). \quad (34)$$

Substituting the finite element approximations into the weak form, we obtain the discrete equilibrium condition as a residual that is expressed at each node (i) (n_{np} is the total number of node points) as

$$\mathbf{r}^{(i)} = \mathbf{r}_{ext}^{(i)} - \mathbf{r}_{int}^{(i)}, \quad i, j = 1 \cdots n_{np}. \quad (35)$$

Here the contributions to the internal and external nodal forces read as

$$\begin{aligned} \mathbf{r}_{int}^{(i)} &= \mathbf{A} \int_{\mathcal{B}_0^e} [\mathbf{F} \cdot \mathbf{S}] \cdot \nabla_{\mathbf{X}} N^{(i)} dV = \mathbf{A} \int_{\mathcal{B}_t^e} \boldsymbol{\sigma} \cdot \nabla_{\mathbf{x}} N^{(i)} dv, \\ \mathbf{r}_{ext}^{(i)} &= \mathbf{A} \int_{\partial \mathcal{B}_0^{e,t}} \mathbf{t}_0^e N^{(i)} dA = \mathbf{A} \int_{\partial \mathcal{B}_t^{e,t}} \mathbf{t}_t^e N^{(i)} da. \end{aligned} \quad (36)$$

The common direct problem is then to determine the deformed shape for a given material configuration, thus the above residual is considered as a (possibly nonlinear) function of the nodal deformation maps

$$\mathbf{r}^{(i)} = \mathbf{r}^{(i)}(\boldsymbol{\varphi}^{(j)}), \quad i, j = 1 \cdots n_{np}. \quad (37)$$

To solve the discrete equilibrium condition (37) numerically with a Newton–Raphson method (see e.g. Bonet and Wood (1997)), we need the tangent stiffness matrix, i.e. the Jacobian matrix of the residual with respect to the nodal deformation maps

$$\mathbf{k}^{(ij)} := - \frac{\partial \mathbf{r}^{(i)}}{\partial \boldsymbol{\varphi}^{(j)}} = \mathbf{A} \int_{\mathcal{B}_0^e} \nabla_{\mathbf{X}} N^{(i)} \cdot \nabla_{\mathbf{X}} N^{(j)} dV. \quad (38)$$

The objective of the less familiar inverse problem is to determine the undeformed shape for a given spatial configuration, thus the above residual is considered as a nonlinear function of the nodal inverse deformation maps

$$\mathbf{r}^{(i)} = \mathbf{r}^{(i)}(\boldsymbol{\Phi}^{(j)}), \quad i, j = 1 \cdots n_{np}. \quad (39)$$

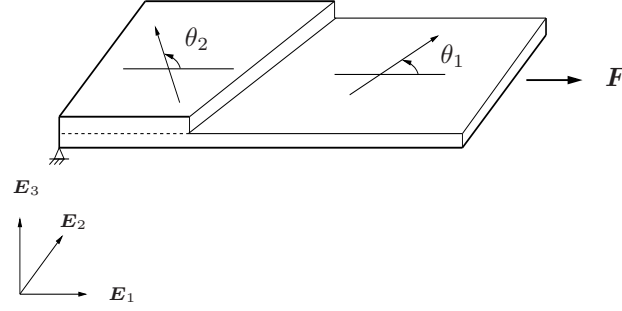


Figure 2: Anisotropic thick sheet under a distributed tension force: deformed shape of straight, rectangular geometry in the spatial configuration \mathcal{B}_t .

Thus the tangent stiffness matrix of the inverse problem follows as the Jacobian matrix of the residual with respect to the nodal inverse deformation maps

$$\mathbf{K}^{(ij)} := -\frac{\partial \mathbf{r}^{(i)}}{\partial \Phi^{(j)}} = \mathbf{A} \int_{\mathcal{B}_t^e} \nabla_{\mathbf{x}} N^{(i)} \mathbb{A} \cdot \nabla_{\mathbf{x}} N^{(j)} \, dv. \quad (40)$$

In the above \mathbb{A} denotes contraction with the second index of the corresponding tangent operator. The implementation renders for both problems quadratic convergence within a Newton solution scheme, as demonstrated in the example section.

7. Examples

The algorithm developed is applied to two benchmark problems: first we analyze the undeformed shape for a three dimensional thick sheet made of two layers of anisotropic material that deforms into a flat rectangular shape under application of a distributed tension force. Thereby we examine the influence of varying anisotropies in the two layers. The second example is concerned with a three dimensional extension of the classical two dimensional Cook's cantilever. Again we seek to determine the undeformed shape for a given anisotropy and a given distributed shear force so that the deformed shape is a straight panel.

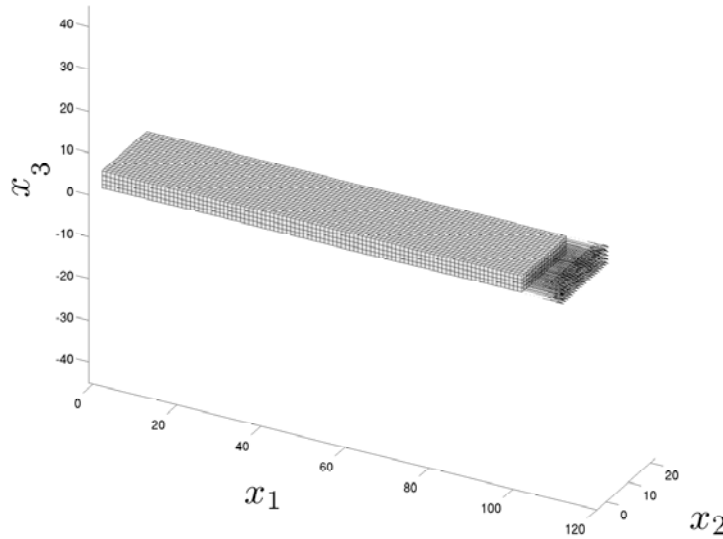
7.1. Anisotropic thick sheet under distributed tension force

The target (straight and rectangular) geometry of the deformed sheet as well as the boundary and loading conditions are visualized in Figure 2. The length of the deformed sheet is set to 100, the width to 20 and the thickness to 4 units of length. The left surface of the thick sheet is fixed in three directions, i.e. fully clamped. A distributed tension load with resultant \mathbf{F} with 400 units of force is applied on the opposite surface in direction of \mathbf{E}_1 . The domain is discretized using trilinear hexahedral finite elements. The deformed, i.e. straight and rectangular sheet is divided in two thick layers in order to attribute different anisotropy directions. We consider a rotation around the fixed laboratory axis \mathbf{E}_3 which rotates \mathbf{E}_1 towards \mathbf{E}_2 in order to obtain the material intrinsic base vectors \mathbf{E}_1^0 and \mathbf{E}_2^0 . The rotation angles θ_1 and θ_2 for the two layers can vary between 0 and 2π . More details on the resulting rotation matrix can be found in the appendix. A material with orthotropic anisotropy in the undeformed shape is considered. Thereby the nine independent variables are comprised of three Young's moduli E_1, E_2, E_3 , the three Poisson's ratios $\nu_{12}, \nu_{13}, \nu_{23}$ and the three shear moduli G_{12}, G_{13}, G_{23} (see the appendix).

In the first example we set the Young's moduli as $E_1=E_2=E_3=2100$, the Poisson ratios as $\nu_{12}=\nu_{13}=\nu_{23}=0.3$ and thus the shear modulus follows as $G_{12}=G_{13}=G_{23}=800$ with $\theta_1=\theta_2=0$ so as to model an isotropic material. Figure 3 shows the deformed shape in the spatial configuration \mathcal{B}_t and Figure 4 the computed undeformed shape in the material configuration \mathcal{B}_0 . As expected the sheet simply elongates without any tendency for bending or twist, thereby we obtain an elongation of 20% in the horizontal direction. Table 1 demonstrates quadratic convergence of the residual norm as a function of iterations using the Newton–Raphson method.

Table 1: Residual norm displaying quadratic convergence.

iteration	norm
1	3.30 E+03
2	1.93 E+03
3	4.39 E+01
4	2.44 E-02
5	4.86 E-07

Figure 3: Discretization of the deformed, i.e. straight, rectangular geometry in the spatial configuration \mathcal{B}_t and distributed tension force.

In the subsequent examples we model anisotropy by selecting the following material parameters

$$\begin{aligned}
 E_1 &= 700 & E_2 &= 2000 & E_3 &= 1000 \\
 \nu_{12} &= 0.3 & \nu_{23} &= 0.3 & \nu_{31} &= 0.3 \\
 G_{12} &= 270 & G_{23} &= 700 & G_{31} &= 400.
 \end{aligned} \tag{41}$$

Furthermore we assign different anisotropy directions to the two layers by setting different values for the rotation angles θ_1 and θ_2 . Figures 5, 6 and 7 display the computed undeformed shape in the material configuration \mathcal{B}_0 for values of $\theta_1 = [0; \pi/2; \pi/4]$ and $\theta_2 = [\pi/4; \pi; 3\pi/4]$, respectively. Again, the convergence of the residual norm as a function of iterations using the Newton–Raphson method is quadratic.

7.2. Anisotropic thick cantilever under distributed shear force

The target geometry of the deformed cantilever as well as the boundary and loading conditions are shown in Figure 8. The dimensions of the thick cantilever in \mathcal{B}_t are $L = 48$, $H_1 = 44$, $H_2 = 16$ and $W = 16$ units of length. Note that these dimensions fit to the classical two dimensional Cook’s membrane benchmark when projected to the $\mathbf{E}_1 - \mathbf{E}_2$ plane, however here we treat a truly three dimensional structure with $W = H_2$. The left side of the thick cantilever is fixed

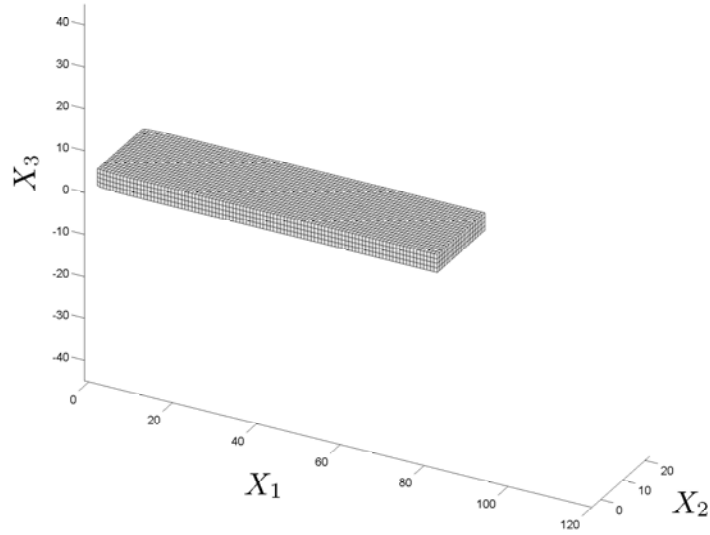


Figure 4: Isotropic material with $\theta_1 = 0$ and $\theta_2 = 0$: computed undeformed shape in the material configuration \mathcal{B}_0 .

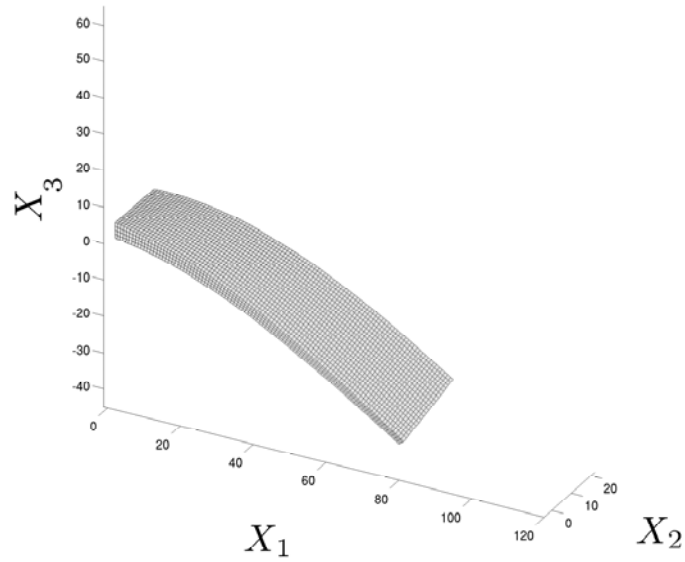


Figure 5: Anisotropic material with $\theta_1 = 0$ and $\theta_2 = \pi/4$: computed undeformed shape in the material configuration \mathcal{B}_0 .

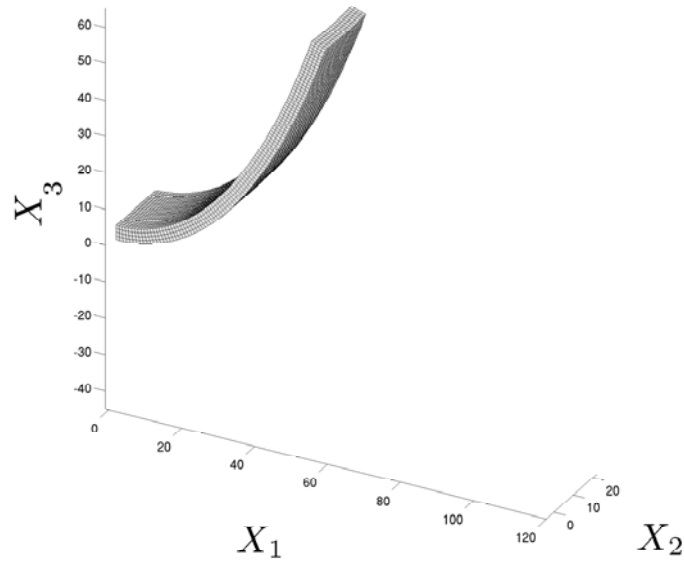


Figure 6: Anisotropic material with $\theta_1 = \pi/2$ and $\theta_2 = \pi$: computed undeformed shape in the material configuration \mathcal{B}_0 .

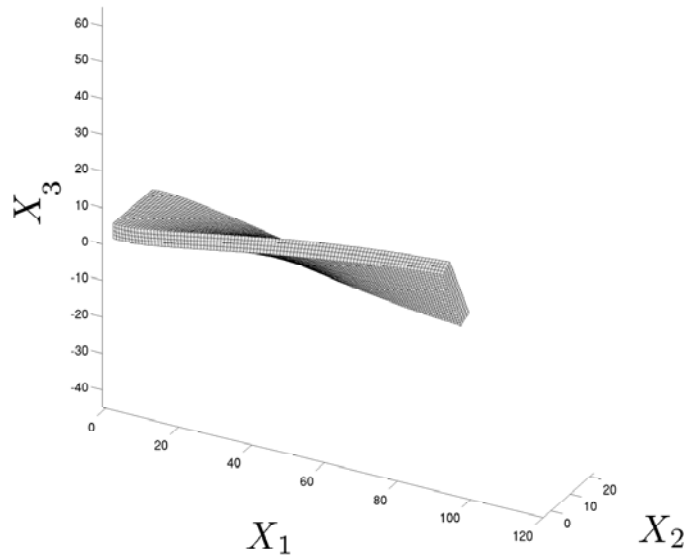


Figure 7: Anisotropic material with $\theta_1 = \pi/4$ and $\theta_2 = 3\pi/4$: computed undeformed shape in the material configuration \mathcal{B}_0 .

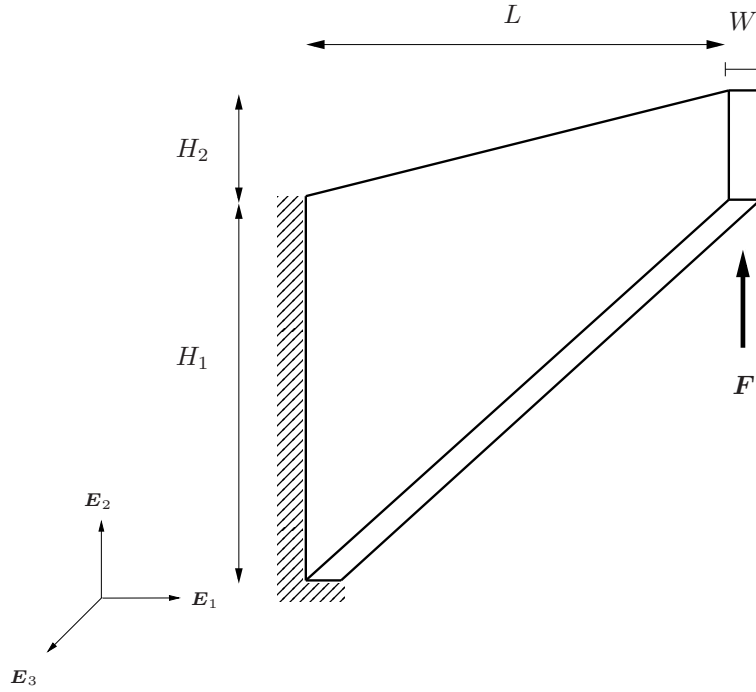


Figure 8: Anisotropic thick cantilever under distributed shear force: deformed shape of panel-line geometry in the spatial configuration \mathcal{B}_t .

in all directions, i.e. it is clamped. The resultant of the applied distributed shear force F is set to 20 units of force. The domain is discretized using trilinear hexahedral finite elements. The anisotropy directions E_I^0 in the undeformed shape are rotated with respect to the fixed laboratory frame E_I , i.e. we consider two orthogonal unit vectors which are defined via the following spherical coordinates: $\theta_{11} = 5\pi/6$, $\theta_{12} = \pi/6$, $\theta_{21} = \pi/3$ and $\theta_{22} = \pi/2$, see the detailed representation of the corresponding rotation matrix in the appendix. An orthotropic material is simulated with the following nine independent material parameters

$$\begin{array}{lll}
 E_1 & = & 700 \\
 \nu_{12} & = & 0.2 \\
 G_{12} & = & 300 \\
 E_2 & = & 200 \\
 \nu_{23} & = & 0.27 \\
 G_{23} & = & 200 \\
 E_3 & = & 500 \\
 \nu_{31} & = & 0.31 \\
 G_{31} & = & 100.
 \end{array} \tag{42}$$

Figures 9, 10 and 11 show the deformed and the computed undeformed shape in the spatial and material configuration \mathcal{B}_t and \mathcal{B}_0 , respectively, as seen in the $E_1 - E_2$ and the $E_1 - E_3$ planes. As expected, the thick cantilever has the largest deformations in the E_2 direction, however, due to the anisotropy, there is also a small contribution in the E_3 direction. The convergence of the residual norm as a function of iterations using the Newton–Raphson method is again quadratic. To confirm the obtained results, the direct problem was re-simulated starting with the coordinates of the previously computed undeformed shape (Figure 10), the same load, boundary conditions and material parameters. The maximum error between the deformed shape obtained with the direct problem and the shape used to compute the undeformed shape (Figure 9) is negligible.

8. Conclusion

This work extends a three dimensional procedure for the determination of the undeformed shape of a workpiece when knowing its desired deformed shape, the boundary conditions and the loads, to the case of anisotropic materials, whereby a logarithmic strain space formulation is used. We simplified the formulation of nonlinear anisotropic hyperelasticity by some mild assumptions, i.e. no body forces are applied, the surface tractions are independent of the inverse deformation mapping and the material is homogeneous. The application of logarithmic strains instead of the common Green–Lagrange

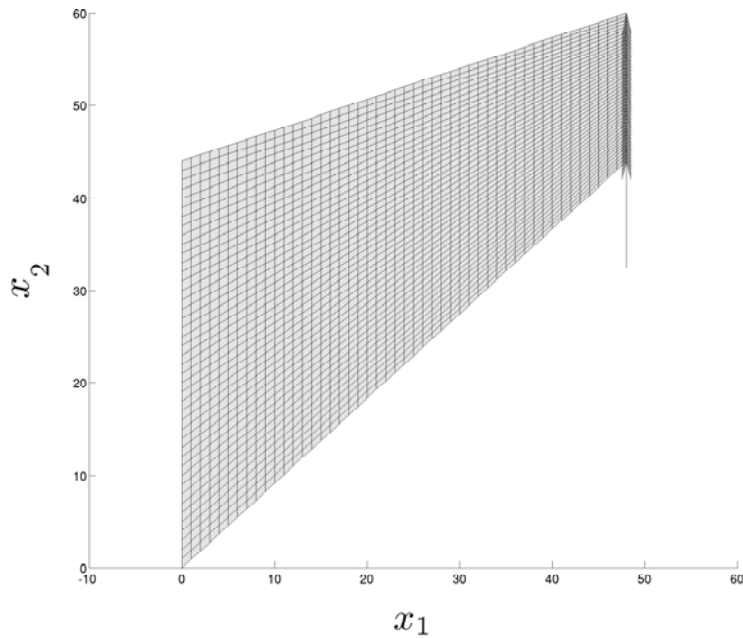


Figure 9: Discretization of the deformed panel-line geometry in the spatial configuration \mathcal{B}_t and distributed shear force (seen in the $\mathbf{E}_1 - \mathbf{E}_2$ plane).

strains makes the consideration of the different anisotropies extremely straightforward in that it mimics the small strain format. Thereby spectral decomposition of the right Cauchy–Green tensor allows a simple evaluation and linearization of the logarithmic strain measure. Two numerical examples in nonlinear orthotropic hyperelasticity illustrate the ability to numerically approximate the undeformed shape, i.e. the question of how an anisotropic specimen must be manufactured in order to obtain the final desired shape upon applying a prescribed load. As a control we verified that the maximum error between the deformed shape obtained with the direct problem and the shape used to compute the undeformed shape is indeed negligible. Future research will be conducted towards the combination between the presented framework and different alternative approaches towards form optimization and towards the extension of the logarithmic strain formulation to plasticity.

Acknowledgement

This work was supported by the German Research Foundation (DFG) under the Transregional Collaborative Research Center SFB/TR73.

Appendix

Anisotropic Elasticities

In the following we shall resort to the Voigt matrix notation for the representation of the fourth-order stiffness tensor \mathbb{E} , the logarithmic (Hencky) strain \mathbf{E} and the auxiliary stress \mathbf{T} . Exploiting symmetry the coefficients of the logarithmic strain \mathbf{E}

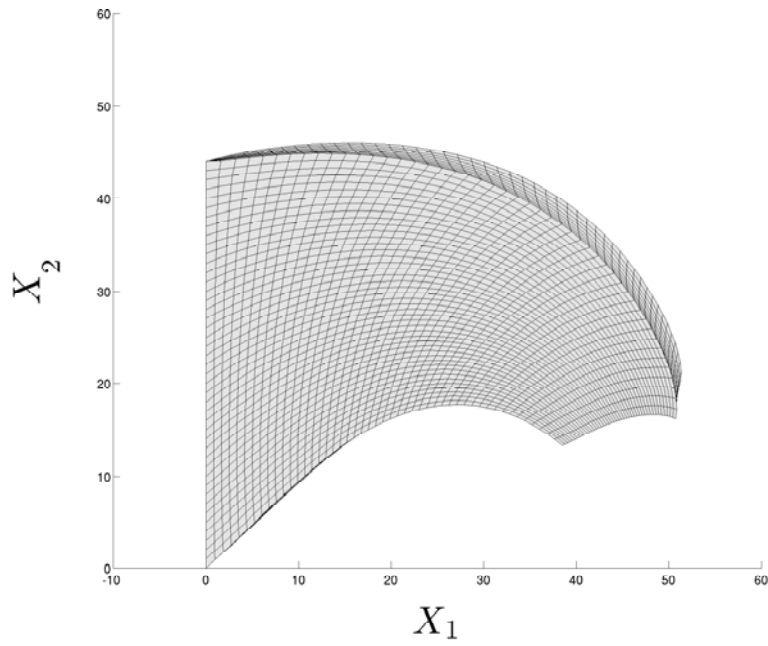


Figure 10: Computed undeformed shape in the material configuration \mathcal{B}_0 (seen in the $\mathbf{E}_1 - \mathbf{E}_2$ plane).

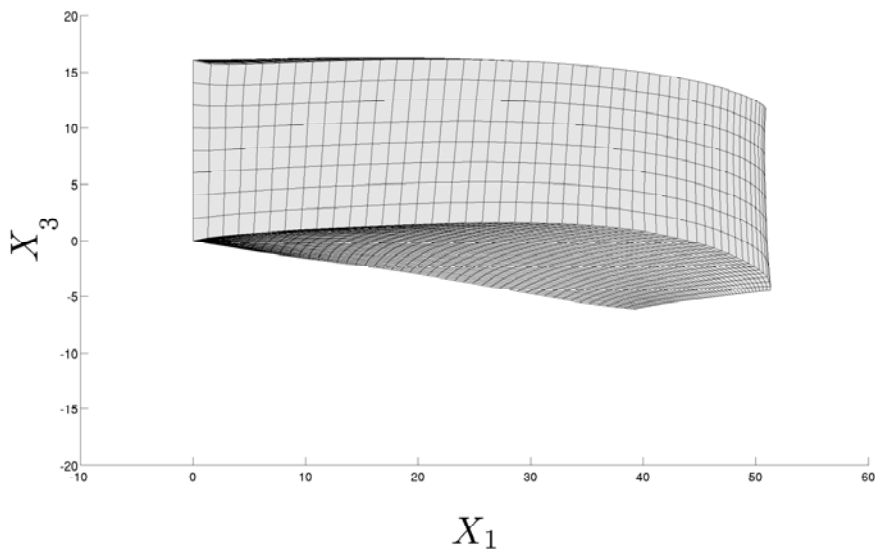


Figure 11: Computed undeformed shape in the material configuration \mathcal{B}_0 (seen in the $\mathbf{E}_3 - \mathbf{E}_1$ plane).

and the auxiliary stress \mathbf{T} are thereby arranged in column matrices \mathbf{e} and \mathbf{t} as

$$\mathbf{e} = \begin{bmatrix} E_{11} \\ E_{22} \\ E_{33} \\ 2E_{(12)} \\ 2E_{(23)} \\ 2E_{(31)} \end{bmatrix}, \quad \mathbf{t} = \begin{bmatrix} T_{11} \\ T_{22} \\ T_{33} \\ T_{(12)} \\ T_{(23)} \\ T_{(31)} \end{bmatrix}. \quad (43)$$

Accordingly, the coefficients of the fourth-order stiffness tensor \mathbb{E} are arranged in a matrix \mathbf{E} as

$$\mathbf{E} = \begin{bmatrix} E_{1111} & E_{1122} & E_{1133} & E_{11(12)} & E_{11(23)} & E_{11(31)} \\ E_{2211} & E_{2222} & E_{2233} & E_{22(12)} & E_{22(23)} & E_{22(31)} \\ E_{3311} & E_{3322} & E_{3333} & E_{33(12)} & E_{33(23)} & E_{33(31)} \\ E_{(12)11} & E_{(12)22} & E_{(12)33} & E_{(12)(12)} & E_{(12)(23)} & E_{(12)(31)} \\ E_{(23)11} & E_{(23)22} & E_{(23)33} & E_{(23)(12)} & E_{(23)(23)} & E_{(23)(31)} \\ E_{(31)11} & E_{(31)22} & E_{(31)33} & E_{(31)(12)} & E_{(31)(23)} & E_{(31)(31)} \end{bmatrix}. \quad (44)$$

Here (ij) denotes symmetrization of indices. A corresponding arrangement into a matrix \mathbf{E}^0 holds for the coefficients of \mathbb{E} with respect to the material intrinsic coordinate system with base vectors \mathbf{E}_M^0 . Summarizing, the following constitutive relation, familiar from the linear elastic small strain setting, holds in Voigt matrix notation

$$\mathbf{t} = \mathbf{E}\mathbf{e}. \quad (45)$$

Anisotropic materials are classified into different symmetry classes such as monoclinic, tetragonal, trigonal, cubic, transversely isotropic, orthotropic, etc. We shall here restrict ourselves to the case of orthotropy, thus the coefficients of the corresponding stiffness tensor with respect to the intrinsic coordinate system follow in the previously introduced Voigt matrix notation as

$$\mathbf{E}^0 = \begin{bmatrix} \frac{1 - \nu_{23}\nu_{32}}{E_2 E_3 \Delta} & \frac{\nu_{21} + \nu_{23}\nu_{31}}{E_2 E_3 \Delta} & \frac{\nu_{31} + \nu_{32}\nu_{21}}{E_2 E_3 \Delta} & 0 & 0 & 0 \\ \frac{E_2 E_3 \Delta}{1 - \nu_{31}\nu_{13}} & \frac{\nu_{32} + \nu_{31}\nu_{12}}{E_3 E_1 \Delta} & \frac{E_3 E_1 \Delta}{1 - \nu_{12}\nu_{21}} & 0 & 0 & 0 \\ \frac{E_3 E_1 \Delta}{E_1 E_2 \Delta} & 0 & 0 & 0 & 0 & 0 \\ SYM & G_{12} & 0 & 0 & 0 & 0 \\ & & G_{23} & 0 & 0 & 0 \\ & & & G_{31} & 0 & 0 \end{bmatrix}. \quad (46)$$

Here the anisotropic stiffness is characterized by nine independent material parameters

$$E_1, E_2, E_3, \nu_{12} = \frac{E_1}{E_2} \nu_{21}, \nu_{23} = \frac{E_2}{E_3} \nu_{32}, \nu_{31} = \frac{E_3}{E_1} \nu_{13}, G_{12}, G_{23}, G_{31}. \quad (47)$$

Thereby E_M denote elasticity moduli in the orthotropy directions \mathbf{E}_M^0 whereas G_{MN} and ν_{MN} denote shear moduli and Poisson ratios in the orthotropy planes spanned by \mathbf{E}_i^0 and \mathbf{E}_j^0 . Moreover, Δ denotes the abbreviation

$$\Delta = \frac{1 - \nu_{12}\nu_{21} - \nu_{23}\nu_{32} - \nu_{31}\nu_{13} - 2\nu_{12}\nu_{23}\nu_{31}}{E_1 E_2 E_3}. \quad (48)$$

Rotation of Base Vectors

In the sequel we shall follow the exposition in Menzel and Steinmann (2001). The material intrinsic base vectors \mathbf{E}_K^0 are given by a forward rotation from the base vectors \mathbf{E}_I of the laboratory coordinate system

$$\mathbf{E}_K^0 = \mathbf{Q} \cdot \mathbf{E}_K = Q_{IK} \mathbf{E}_I, \quad \text{with} \quad \mathbf{Q} = Q_{IJ} \mathbf{E}_I \otimes \mathbf{E}_J = \mathbf{E}_J^0 \otimes \mathbf{E}_J. \quad (49)$$

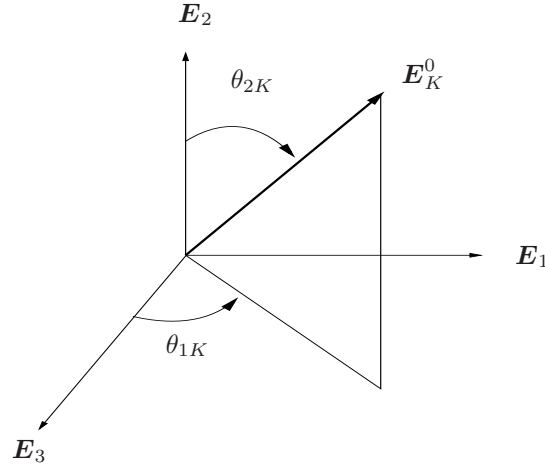


Figure 12: Spherical coordinates.

Here Q_{IJ} denote the coefficients of the rotation tensor \mathbf{Q} in the laboratory coordinate system. In spherical coordinates Q_{IJ} may be expressed in terms of two angles θ_{1K} and θ_{2K} for each base vector $\mathbf{E}_K^0 = Q_{IK}\mathbf{E}_I$ (Figure 12) such that

$$[Q_{IK}] = \begin{bmatrix} \sin\theta_{11}\sin\theta_{21} & \sin\theta_{12}\sin\theta_{22} & \sin\theta_{13}\sin\theta_{23} \\ \cos\theta_{21} & \cos\theta_{22} & \cos\theta_{23} \\ \cos\theta_{11}\sin\theta_{21} & \cos\theta_{12}\sin\theta_{22} & \cos\theta_{13}\sin\theta_{23} \end{bmatrix}. \quad (50)$$

Clearly, the angles θ_{1K} and θ_{2K} may not be chosen independently for $K = 1, 2, 3$ but have to satisfy the orthonormality conditions $\mathbf{E}_K^0 \cdot \mathbf{E}_L^0 = [Q_{IK}\mathbf{E}_I] \cdot [Q_{JL}\mathbf{E}_J] = Q_{IK}Q_{JL} = \delta_{KL}$. Finally the transformation of the coefficients of the stiffness tensor due to the rotation of basis vectors as given by $R_{IJKL} = Q_{IM}Q_{JN}$, i.e.

$$E_{IJKL} = R_{IJKL} E_{MNO}^0 R_{KLOP} \quad (51)$$

is expressed in Voigt matrix notation as

$$\mathbf{R} = \begin{bmatrix} Q_{11}^2 & Q_{12}^2 & Q_{13}^2 & 2Q_{11}Q_{12} & 2Q_{12}Q_{13} & 2Q_{13}Q_{11} \\ Q_{21}^2 & Q_{22}^2 & Q_{23}^2 & 2Q_{21}Q_{22} & 2Q_{22}Q_{23} & 2Q_{23}Q_{21} \\ Q_{31}^2 & Q_{32}^2 & Q_{33}^2 & 2Q_{31}Q_{32} & 2Q_{32}Q_{33} & 2Q_{33}Q_{31} \\ Q_{11}Q_{21} & Q_{12}Q_{22} & Q_{13}Q_{23} & Q_{11}Q_{22} + Q_{12}Q_{21} & Q_{12}Q_{23} + Q_{13}Q_{22} & Q_{13}Q_{21} + Q_{11}Q_{23} \\ Q_{21}Q_{31} & Q_{22}Q_{32} & Q_{23}Q_{33} & Q_{21}Q_{32} + Q_{22}Q_{31} & Q_{22}Q_{33} + Q_{23}Q_{32} & Q_{23}Q_{31} + Q_{21}Q_{33} \\ Q_{31}Q_{11} & Q_{32}Q_{12} & Q_{33}Q_{13} & Q_{31}Q_{12} + Q_{32}Q_{11} & Q_{32}Q_{13} + Q_{33}Q_{12} & Q_{33}Q_{11} + Q_{31}Q_{13} \end{bmatrix}. \quad (52)$$

The coefficients of the stiffness tensor in Voigt matrix notation thus follow as

$$\mathbf{E} = \mathbf{R}\mathbf{E}^0\mathbf{R}^t. \quad (53)$$

As an example for the simple case of a counter-clockwise rotation with angle θ around the \mathbf{E}_3 axis of the laboratory coordinate system, i.e. $\theta_{1\beta} = \pi/2$, $\theta_{21} = \pi/2 - \theta$, $\theta_{22} = -\theta$, we obtain for the rotation coefficients in matrix notation

$$\mathbf{Q} = [Q_{IJ}] = \begin{bmatrix} +\cos\theta & -\sin\theta & 0 \\ +\sin\theta & +\cos\theta & 0 \\ 0 & 0 & 1 \end{bmatrix}. \quad (54)$$

The transformation matrix \mathbf{R} then reduces to

$$\mathbf{R} = \begin{bmatrix} \cos^2\theta & \sin^2\theta & 0 & -2\cos\theta\sin\theta & 0 & 0 \\ \sin^2\theta & \cos^2\theta & 0 & +2\cos\theta\sin\theta & 0 & 0 \\ 0 & 0 & 1 & 0 & 0 & 0 \\ \cos\theta\sin\theta & -\cos\theta\sin\theta & 0 & \cos^2\theta - \sin^2\theta & 0 & 0 \\ 0 & 0 & 0 & 0 & +\cos\theta & +\sin\theta \\ 0 & 0 & 0 & 0 & -\sin\theta & +\cos\theta \end{bmatrix}. \quad (55)$$

References

- Bonnet J., Wood R.D. (1997) 'Non linear continuum mechanics for finite element analysis', *Cambridge University Press*.
- Fachinotti V.D., Cardona A., Jetteur P. (2008) 'Finite element modelling of inverse design problems in large deformations anisotropic hyperelasticity', *Int. J. Numer. Meth. Engng.*, Vol. 74, pp.894–910.
- Govindjee S., Mihalic P.A. (1996) 'Computational methods for inverse finite elastostatics', *Comp. Meth. Appl. Mech. Engrg.*, Vol. 136, pp.47–57.
- Govindjee S., Mihalic P.A. (1998) 'Computational methods for inverse deformations in quasi-incompressible finite elasticity', *Int. J. Num. Meth. Engrg.*, Vol. 43, pp.821–838.
- Govindjee S. (1999) 'Finite Deformation Inverse Design Modeling with Temperature Changes, Axis-Symmetry and Anisotropy', *UCB/SEMM-1999/01*, University of California Berkeley.
- Koishi M., Govindjee S. (2001) 'Inverse Design Methodology of a tire', *Tire Science and Technology Journal*, Vol. 29, pp.155–170.
- Menzel A., Steinmann P. (2001) 'On the Comparison of Two Strategies to Formulate Orthotropic Hyperelasticity', *Journal of Elasticity*, Vol. 62, pp.171–201.
- Miehe C. (1993) 'Computation of isotropic tensor functions', *Communications in numerical methods in engineering*, Vol. 9, pp.889–896.
- Miehe C., Lambrecht M. (2001) 'Algorithms for computation of stresses and elasticity moduli in terms of Seth-Hill's family of generalized strain tensors', *Communications in numerical methods in engineering*, Vol. 17, pp.337–353.